3
Membrane Material Models

Membrane structures have a lot of material possibilities. Some membrane materials are reported in Krishna[48]: reinforced fiber with glass or plastic, wooden board, concrete plate and a vast variety of fabrics. Lewis[49] shows in his work that the materials most used are: PVC coated with polyester, teflon coated with glass fiber and canvas. Elias [50] adds to this list the materials: kevlar®(para-aramid synthetic fiber), nylon, polytetrafluoretileno (PTFE) and silicon. A material that recently finds application specifically to pneumatic structures is the ethylene tetrafluoroethylene (ETFE).

To comprehend the huge variety of materials available for membrane and pneumatic structures, several models for material behavior are presented in this chapter. All the material model formulations presented here were implemented in the research program CARAT++ [51]. Validation examples of these models are also presented.

3.1
Small strains — Elastoplasticity

Small strains or infinitesimal strains theory deals with infinitesimal deformations of a body. Elastoplastic and elastoviscoplastic material models considering small strains will be described.

The formulation used for the elastoplastic material is classic and it is presented for instance in the studies of Simo and Taylor [52], Simo and Hughes [39], and Souza Neto et al.[40].

The total strain $\mathbf{E}$ splits into a elastic strain $\mathbf{E}^e$ and a plastic strain $\mathbf{E}^p$:

$$\mathbf{E} = \mathbf{E}^e + \mathbf{E}^p \tag{3-1}$$

The elastic constitutive law considering linear elasticity is given by the relation:

$$\mathbf{S} = \mathbf{D} : (\mathbf{E} - \mathbf{E}^p) \tag{3-2}$$

where $\mathbf{D}$ is the elastic moduli tensor. The yield condition is given by the function:

$$f(\mathbf{S}, q) = \phi(\mathbf{S}) + q(\sigma_y, K) \leq 0 \tag{3-3}$$

where σ_y is the yield stress and K is the hardening modulus. If $K < 0$, one speaks of a softening response.

The flow rule and the hardening law in associative plasticity models is given respectively by:

$$\dot{\boldsymbol{E}}_{\boldsymbol{p}} = \gamma \frac{\partial f}{\partial \mathbf{S}} \tag{3-4}$$

$$\dot{\boldsymbol{\alpha}} = \gamma \frac{\partial f}{\partial q} \tag{3-5}$$

where γ is the consistency parameter, $\frac{\partial f}{\partial \mathbf{S}}$ is a function that defines the direction of plastic flow, and $\frac{\partial f}{\partial q}$ is a function that describes the hardening evolution.

The actual state $(\mathbf{S}, q)$ of stress and hardening force is a solution to the following constrained optimization problem:

$$\begin{aligned} &maximise \quad \mathbf{S} : \dot{\mathbf{E}} - q \cdot \dot{\alpha} \\ &subject\ to \quad f(\mathbf{S}, q) \leq 0 \end{aligned} \tag{3-6}$$

Solution for the problem 3-6 satisfies the Kuhn-Tucker optimality conditions, the so called loading/unloading condition.

$$\gamma \geq 0, \qquad f(\mathbf{S}, q) \leq 0, \qquad \gamma f(\mathbf{S}, q) = 0 \tag{3-7}$$

3.1.1
Plane Stress

In the present work membrane structures are analyzed, therefore all material models are implemented considering plane stress conditions.

Figure 3.1 shows the plane stress state, where the stresses S_{13}, S_{23}, and S_{33} are zero. The stress tensor is given by

$$\mathbf{S} = \begin{bmatrix} S_{11} & S_{12} & 0 \\ S_{21} & S_{22} & 0 \\ 0 & 0 & 0 \end{bmatrix} \tag{3-8}$$

The stress tensor can be written in voigt-notation as:

$$\mathbf{S} = \begin{bmatrix} S_{11} & S_{22} & S_{12} \end{bmatrix} \tag{3-9}$$

The components E_{ij} of the total strain tensor $\mathbf{E}$ are correspondingly:

$$\mathbf{E} = [E_{11}\ E_{22}\ 2E_{12}]$$

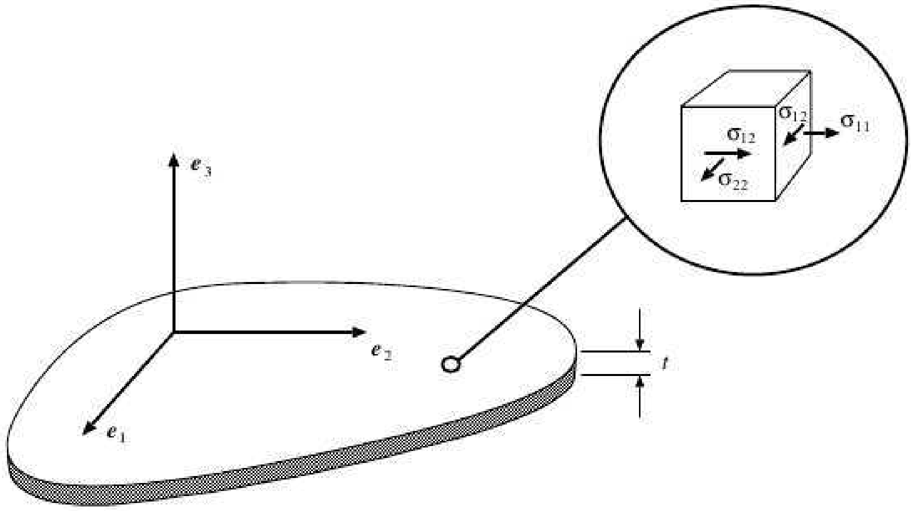

Figure 3.1: Plane stress state (source: Souza Neto et al. [40])

3.1.2
Von Mises yield criteria - Plane Stress

Figure 3.2 presents the experimental data from uniaxial and biaxial test of ETFE from works of Moritz [15], Galliot and Luchsinger [53], and DuPONT^{TM} Tefzel® [54] and an adjusted von Mises yield curve. This yield surface was generated considering an yield stress of $16MPa$. Figure 3.2 shows that the von Mises criteria is a good approximation for the experimental data for the ETFE material.

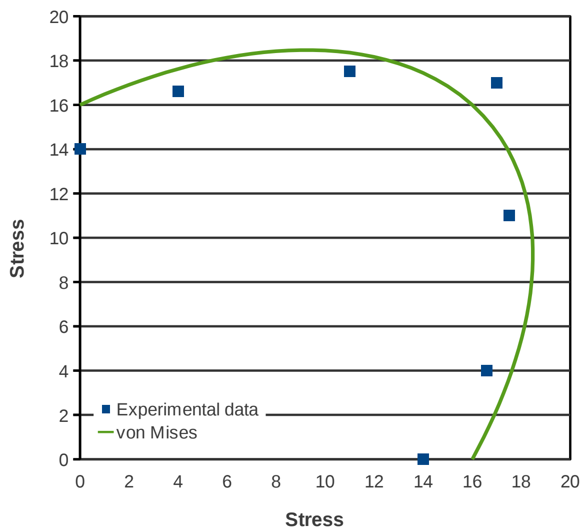

Figure 3.2: Experimental data from uniaxial and biaxial test of ETFE and adjusted von Mises yield curve

The von Mises yield criteria suggests that yielding begins when $J2$, the second invariant of the deviatoric stress, reaches a critical value (k) [55].

$$f(J2) = \sqrt{J2} - k = 0 \quad \leftrightarrow \quad f(J2) = J2 - k^2 = 0 \tag{3-10}$$

In vector notation the deviatoric stress **s** is written:

$$\mathbf{s} = [s_{11}\ \ s_{22}\ \ s_{12}] \tag{3-11}$$

which can be obtained by the projection of the stress tensor on the deviatoric plane.

$$\mathbf{s} = dev[\mathbf{S}] = \bar{\mathbf{P}}\mathbf{S} \qquad \bar{\mathbf{P}} = \frac{1}{3}\begin{bmatrix} 2 & -1 & 0 \\ -1 & 2 & 0 \\ 0 & 0 & 3 \end{bmatrix} \tag{3-12}$$

$J2$ is calculated through:

$$J2 = \mathbf{SPS} \tag{3-13}$$

Similarly the elastic and plastic strain tensors ($\mathbf{E}^e$, $\mathbf{E}^p$) are collected in vector form as:

$$\mathbf{E}^e = [E_{11}^e\ \ E_{22}^e\ \ 2E_{12}^e] \qquad \mathbf{E}^p = \left[E_{11}^p\ \ E_{22}^p\ \ 2E_{12}^p\right]$$

and the deviatoric strain is given by:

$$\mathbf{e} = dev[\mathbf{E}] = \mathbf{PE} \qquad \mathbf{P} = \frac{1}{3}\begin{bmatrix} 2 & -1 & 0 \\ -1 & 2 & 0 \\ 0 & 0 & 6 \end{bmatrix} \tag{3-14}$$

Linear isotropic hardening is considered, for which the scalar hardening state variable is:

$$q = \sigma_y + K\alpha \tag{3-15}$$

where α is the amount of plastic flow and K is a hardening material parameter.

The von Mises yield function for plane stress following 3-10 is:

$$f(\mathbf{S},\alpha) = \sqrt{\mathbf{S}^T\mathbf{PS}} - \sqrt{\frac{2}{3}}q(\alpha) \quad \leftrightarrow \quad f(\mathbf{S},\alpha) = \frac{1}{2}\mathbf{S}^T\mathbf{PS} - \frac{1}{3}(q(\alpha))^2 \tag{3-16}$$

$$f(\mathbf{S},\alpha) = \mathbf{SPS} - \sqrt{\frac{2}{3}} \cdot \sqrt{\mathbf{S}^T\mathbf{PS}} \cdot q(\alpha)$$

From the above expression, equations 3-4 and 3-5 result in:

$$\dot{\mathbf{E}}^p = \gamma\frac{\partial f}{\partial \mathbf{S}} = \gamma\mathbf{PS} \tag{3-17}$$

$$\dot{\alpha} = \gamma \frac{\partial f}{\partial q} = \gamma \sqrt{\frac{2}{3}\mathbf{S}^T\mathbf{PS}} \tag{3-18}$$

With these equations the J2 plasticity model with isotropic hardening for plane stress condition is summarized:

$$\boxed{\begin{gathered} \mathbf{E} = \mathbf{E}^e + \mathbf{E}^p \\ \mathbf{S} = \mathbf{D}\mathbf{E}^e \\ \dot{\mathbf{E}} = \gamma\mathbf{PS} \\ f = \tfrac{1}{2}\mathbf{SPS} - \tfrac{1}{3}(K\alpha)^2 \\ \dot{\alpha} = \gamma\sqrt{\tfrac{2}{3}\mathbf{S}^T\mathbf{PS}} \end{gathered}} \tag{3-19}$$

where **D** is the linear elastic constitutive matrix for plane stress defined as:

$$\mathbf{D} = \frac{E}{1-\nu^2}\begin{bmatrix} 1 & \nu & 0 \\ \nu & 1 & 0 \\ 0 & 0 & \frac{1-\nu}{2} \end{bmatrix} \tag{3-20}$$

where ν is the Poisson ratio and E is the elastic modulus.

The updating scheme for integration of the corresponding rate constitutive equations requires the formulation of a numerical algorithm. The implicit Euler or backward scheme is used to discretize the incremental constitutive problem. Based in equations 3-19 the resulting equations with the implicit Euler follow:

$$f_{n+1}(\Delta\gamma) = \frac{1}{2}\bar{f} - \frac{1}{3}R^2 \tag{3-21}$$

$$\bar{f} = \frac{1}{6}\frac{\left(S_{11}^{trial} + S_{22}^{trial}\right)^2}{\left(1 + \frac{E\Delta\gamma}{3-3\nu}\right)^2} + \frac{1}{2}\frac{\left(S_{11}^{trial} - S_{22}^{trial}\right)^2 + (S_{21}^{trial})^2}{\left(1 + \frac{E\Delta\gamma}{1+\nu}\right)^2} \tag{3-22}$$

$$R^2 = \left(\sigma_y + \alpha_{n+1}K\right)^2 = \left[\sigma_y + \left(\alpha_n + \Delta\gamma\sqrt{\frac{2}{3}}\sqrt{\mathbf{S}_{n+1}^T\mathbf{PS}_{n+1}}\right)K\right]^2 \tag{3-23}$$

$$\mathbf{E}_{n+1}^p = \mathbf{E}_n^p + \Delta\gamma\mathbf{PS}_{n+1} \tag{3-24}$$

$$\alpha_{n+1} = \alpha_n + \Delta\gamma\sqrt{\frac{2}{3}}\sqrt{\mathbf{S}_{n+1}^T\mathbf{PS}_{n+1}} \tag{3-25}$$

$$\mathbf{S}_{n+1}^{trial} = \mathbf{D}[\mathbf{E}_{n+1} - \mathbf{E}_n^p] \tag{3-26}$$

$$\mathbf{S}_{n+1} = \mathbf{\Xi}(\Delta\gamma)\mathbf{D}^{-1}\mathbf{S}_{n+1}^{trial} \tag{3-27}$$

$$\mathbf{\Xi}(\Delta\gamma) = \left[\mathbf{D}^{-1} + \Delta\gamma\mathbf{P}\right]^{-1} \tag{3-28}$$

The consistent elastoplastic tangent moduli is obtained with equations 3-29 and 3-30. For more details of the computation of the consistent elastoplastic tangent moduli we refer to Simo and Hughes [39].

$$\left.\frac{d\mathbf{S}}{d\mathbf{E}}\right|_{n+1} = \boldsymbol{\Xi} - \frac{[\boldsymbol{\Xi}\mathbf{P}\mathbf{S}_{n+1}][\boldsymbol{\Xi}\mathbf{P}\mathbf{S}_{n+1}]}{\mathbf{S}_{n+1}\mathbf{P}\boldsymbol{\Xi}\mathbf{P}\mathbf{S}_{n+1} + \beta_{n+1}} \tag{3-29}$$

$$\beta_{n+1} = \frac{2}{3}\frac{\left(K\mathbf{S}_{n+1}^{T}\mathbf{P}\mathbf{S}_{n+1}\right)}{\left(1 - \frac{2}{3}K\Delta\gamma\right)} \tag{3-30}$$

The return mapping is the closest point projection (Simo and Hughes [39]). This return mapping considers a two-step algorithm called the elastic predictor/plastic corrector algorithm. This algorithm assumes that the first step is elastic, which is called as the elastic trial solution ($\mathbf{S}_{n+1}^{trial}$). If this elastic trial stress violates the yield function (equation 3-16) a new solution must be obtained with the plastic corrector step. The elastic predictor/plastic corrector algorithm has a geometric interpretation as can be seen in Figure 3.3. The plastic corrector step and the implementation of the return mapping are presented in boxes 3.1 and 3.2. These algorithms are based in the works of Simo and Taylor[52] and Souza Neto et. ali.[40].

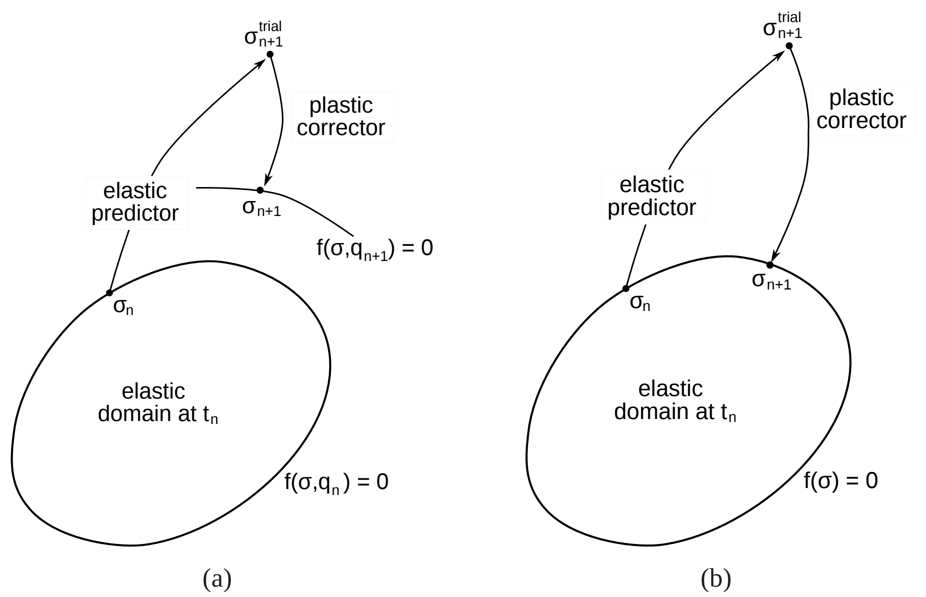

Figure 3.3: General return mapping schemes. Geometric interpretation: (a) hardening plasticity and (b) perfect plasticity (source: Souza Neto et al.[40])

The plastic multiplier ($\Delta(\gamma)$) is solved using the Newton-Raphson procedure because of the nonlinear equations in $\Delta(\gamma)$. The Newton-Raphson procedure is presented in box 3.2.

1. Update the deformation tensor and compute the trial elastic stress and yield function for trial state.
$$\mathbf{E}_{n+1} = \mathbf{E}_n + \nabla^S u$$
$$\mathbf{S}^{trial}_{n+1} = \mathbf{D}[\mathbf{E}_{n+1} - \mathbf{E}^p_n]$$
$$f(\Delta\gamma) = \frac{1}{2}\bar{f} - \frac{1}{3}R^2 \quad \Delta\gamma = 0$$

2. **If** $f(\Delta\gamma) \leq 0$
then set $(.)_{n+1} = (.)^{trial}_{n+1}$ and **exit**

3. Solve $f(\Delta\gamma) = 0$ for $\Delta\gamma$ using the Newton-Raphson method - go to box 3.2

4. Compute the algorithmic tangent moduli
$$\mathbf{\Xi} = \left[\mathbf{D}^{-1} + \Delta\gamma\mathbf{P}\right]^{-1}$$

5. Update the stress and plastic strain in t_{n+1}
$$\mathbf{S}_{n+1} = \mathbf{\Xi}(\Delta\gamma)\mathbf{D}^{-1}\mathbf{S}^{trial}_{n+1}$$
$$\alpha_{n+1} = \alpha_n + \Delta\gamma\sqrt{\frac{2}{3}}\sqrt{\mathbf{S}^T_{n+1}\mathbf{P}\mathbf{S}_{n+1}}$$
$$\mathbf{E}^p_{n+1} = \mathbf{E}^p_n + \Delta\gamma\mathbf{P}\mathbf{S}_{n+1}$$

6. Compute the consistent elastoplastic tangent moduli
$$\left.\frac{d\mathbf{S}}{d\mathbf{E}}\right|_{n+1} = \mathbf{\Xi} - \frac{[\mathbf{\Xi}\mathbf{P}\mathbf{S}_{n+1}][\mathbf{\Xi}\mathbf{P}\mathbf{S}_{n+1}]}{\mathbf{S}_{n+1}\mathbf{P}\mathbf{\Xi}\mathbf{P}\mathbf{S}_{n+1} + \beta_{n+1}}$$
$$\beta_{n+1} = \frac{2}{3}\frac{\left(K\mathbf{S}^T_{n+1}\mathbf{P}\mathbf{S}_{n+1}\right)}{\left(1 - \frac{2}{3}K\Delta\gamma\right)}$$

7. Update $\mathbf{E}_{33}$
$$E_{33n+1} = -\frac{\nu}{E}(S_{11n+1} + S_{22n+1}) - (E^p_{11n+1} + E^p_{22n+1})$$

Box 3.1: Algorithm for the elastoplastic material

1. Set initial guess for $\Delta\gamma$

$$\Delta\gamma = 0$$

$$f(\Delta\gamma) = \frac{1}{2} \cdot \bar{f}(\Delta\gamma) - \frac{1}{3}R^2(\Delta\gamma) = 0$$

2. Perform Newton-Raphson iteration

$$\bar{f}' = -\frac{1}{3}\frac{\left(S_{11}^{trial} + S_{22}^{trial}\right)^2 E}{\left(1 + \frac{E\Delta\gamma}{3-3\nu}\right)^3 (3-3\nu)} - \frac{\left(\left(S_{11}^{trial} - S_{22}^{trial}\right)^2 + 4S_{21}^{trial2}\right)E}{\left(1 + \frac{E\Delta\gamma}{1+\nu}\right)^3 (1+\nu)}$$

$$R^{2'} = 2\sigma_y\left(\alpha_n + \Delta\gamma\sqrt{\frac{2}{3}\bar{f}}\right)K\sqrt{\frac{2}{3}}\left(\sqrt{\bar{f}} + \frac{\Delta\gamma\bar{f}'}{2\sqrt{\bar{f}}}\right)$$

$$f' = \frac{1}{2}\bar{f}' - \frac{1}{3}R^{2'}$$

$$\Delta\gamma_{n+1} = \Delta\gamma_n - \frac{f}{f'}$$

3. Check for convergence if $\Delta\gamma_{n+1} - \Delta\gamma_n \leq tol$ then return to box 3.1 else go to 1

Box 3.2: Newton–Raphson algorithm to solve $\Delta\gamma$

3.1.3
Benchmark Example

The stretching of a perforated rectangular membrane along the longitudinal axis is presented as a benchmark example to evaluate the implementation described above. This example is taken from Simo and Hughes [39], Simo and Taylor [56], and Souza Neto et al. [40] and is modeled in CARAT++ for plane stress with membrane elements. The material is elastoplastic with isotropic hardening and von Mises yield criteria.

The membrane material properties are: $E = 70GPa$ (membrane modulus), $\nu = 0.2$ (Poisson ratio), $K = 0.2GPa$ (hardening modulus), $\sigma_y = 0.243GPa$ (yielding stress), and membrane thickness of 1 mm. The dimension and boundary conditions are shown in figure 3.4. The static analysis was carried out with cylindrical arc-length control of the free edge. The mesh is composed of 531 nodes and 480 quadrilateral linear membrane elements as shown in figure 3.4. Due to symmetry a quarter of the geometry is modeled.

Figure 3.5 presents the results for the total applied force versus displacement on the membrane free edge. The results are in accordance with Souza Neto et al. [40].

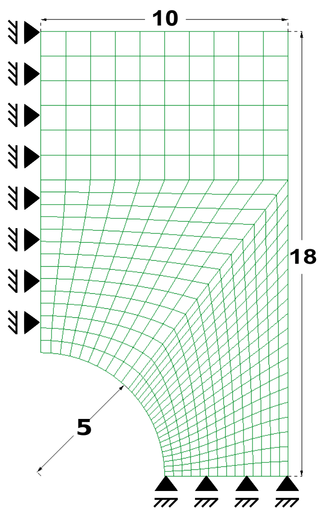

Figure 3.4: Mesh, geometry and boundary conditions of a perforated rectangular membrane

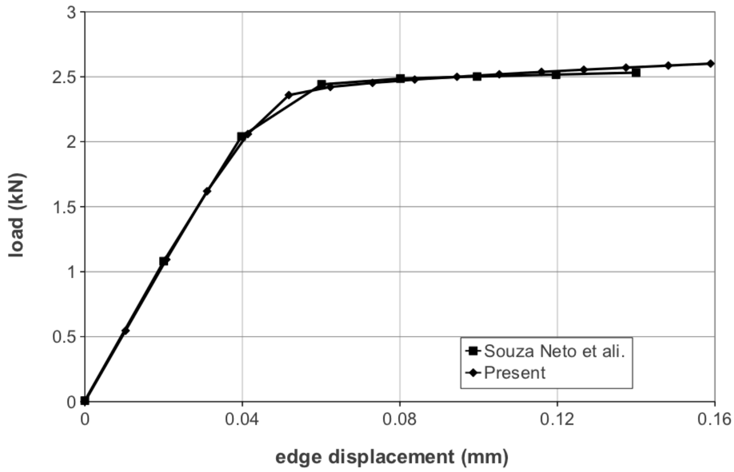

Figure 3.5: Load versus edge displacement

3.2
Small strains — Elastoviscoplasticity

The elastoviscoplastic material model reflects the plastic deformation dependence with time. The temperature is often related with this phenomena.

According to Souza Neto et al. [40], materials such as metals, rubbers, geomaterials in general, concrete and composites may all present substantial time-dependent mechanical behavior.

The phenomenological aspects for elastoviscoplasticity are: strain rate dependence, creep and relaxation.

The strain rate dependence is observed when a material is subjected to tests carried out under different prescribed strain rates. According to Souza Neto et al. [40], the elasticity modulus is mostly independent of the rate of loading but, the initial yield limit as well as the hardening curve depend strongly on the rate of straining. This rate-dependence is also observed at low temperatures, but usually becomes significant only at higher temperatures. In figure 3.6(a) the phenomenological aspects of the strain rate dependence is presented.

Creep is the phenomenon by which that at a constant stress condition the strain increases. For different levels of stress the response for strain is also different. This is shown in figure 3.6(b). Souza Neto et al. [40] reports that high strain rates shown towards the end of the schematic curves for high and moderate stresses is the phenomenon known as tertiary creep. Tertiary creep leads to the final rupture of the material and is associated with the evolution of internal damage.

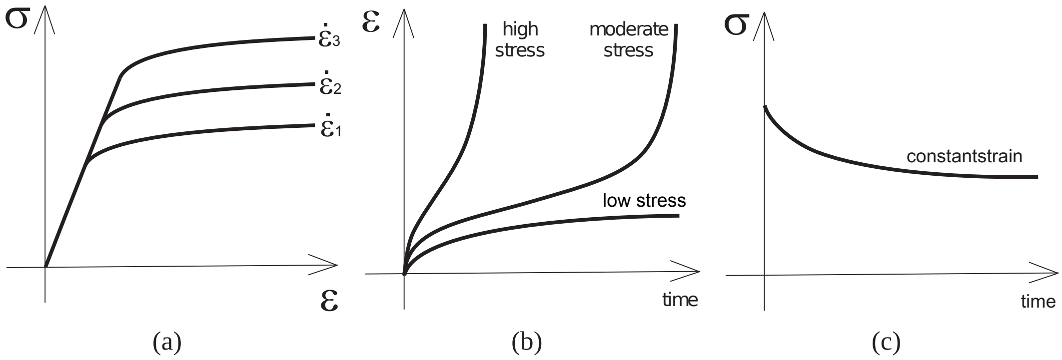

Figure 3.6: Phenomenological aspects: uniaxial tensile tests at high temperature (a) Strain rate dependence, (b) Creep, and (c) Relaxation (source: Souza Neto et al. [40])

Relaxation occurs when by a constant strain stress decays in time. This phenomenon is depicted in figure 3.6(c)

The viscoplastic flow rule is defined as:

$$\dot{\mathbf{E}}^{vp} = \gamma \frac{\partial f}{\partial \mathbf{S}} \tag{3-31}$$

The explicit function for γ models how the rate of plastic straining varies with the level of stress. There are many models to describe γ. Souza Neto et al. [40] reports that a particular choice should be dictated by its ability to model the dependence of the plastic strain rate on the state of stress for the material under consideration.

Some models for the viscoplastic strain are described next.

3.2.1 Perzyna Model

This model was introduced by Perzyna (apud Souza Neto et al. [40])) and is widely used in computational applications of viscoplasticity. It is defined by:

$$\gamma(S,\sigma_y) = \frac{< f_{n+1} >}{\mu} \tag{3-32}$$

$$< f_{n+1} >= \begin{cases} \left[\frac{J2(S)}{q} - 1\right]^{1/\epsilon} & if \quad f(S,\sigma_y) \geq 0 \\ 0 & if \quad f(S,\sigma_y) < 0 \end{cases} \tag{3-33}$$

where μ is the viscosity–related parameter, whose dimension is time and the rate-sensitivity ϵ is a non-dimensional parameter. Both parameters are strictly positive and temperature dependent. According to Souza Neto et al. [40], as a general rule, as temperature increases (decreases) μ and ϵ increases (decreases).

3.2.2 Perić Model

This form has been introduced by Peric (apud Souza Neto et al. [40]) and is given by:

$$< f_{n+1} >= \begin{cases} \left[\left(\frac{J2(S)}{q}\right)^{1/\epsilon} - 1\right] & if \quad f(S,\sigma_y) \geq 0 \\ 0 & if \quad f(S,\sigma_y) < 0 \end{cases} \tag{3-34}$$

Souza Neto et al. [40] reports that in spite of its similarity to Perzyna's definitions, as the rate-independent limit is approached with vanishing rate-sensitivity $\epsilon \to 0$, the Perzyna model does not reproduce the uniaxial stress-strain curve of the corresponding rate–independent model with yield stress σ_y. As shown by Perić, in this limit, the Perzyna model produces a curve with $S = 2\sigma_y$ instead. However, for vanishing viscosity ($\mu \to 0$) or vanishing strain rates, the response of both Perzyna and Perić models coincide with the standard rate-independent model with yield stress σ_y.

The implementation of the present elastoviscoplastic material model follows the algorithm presented in section 3.1 (see boxes 3.1 and 3.2), modifying $\Delta\gamma$ to include the time parameter:

$$\Delta\gamma = \Delta t \cdot \gamma =< f_{n+1} > \frac{\Delta t}{\mu}, \qquad \mu \in (0,\infty) \tag{3-35}$$

where Δt is time increment.

1. Update the deformation tensor and compute the trial elastic stress.

$$\mathbf{E}_{n+1} = \mathbf{E}_n + \nabla^S u \tag{3-36}$$

$$\mathbf{S}^{trial}_{n+1} = \mathbf{D}[\mathbf{E}_{n+1} - \mathbf{E}^{vp}_n] \tag{3-37}$$

$$f(\Delta\gamma) = \frac{1}{2}\bar{f} - \frac{1}{3}R^2 \tag{3-38}$$

2. Solve $f(\Delta\gamma) = 0$ for $\Delta\gamma$ using the Newton–Raphson method — go to box 3.4
3. Compute the algorithm tangent moduli

$$\mathbf{\Xi} = \left[\mathbf{D}^{-1} + \Delta\gamma\mathbf{P} + \frac{\partial\Delta\gamma}{\partial\mathbf{S}_{n+1}} \otimes \mathbf{P}\mathbf{S}_{n+1}\right]^{-1} \tag{3-39}$$

4. Update the stress and plastic strain in t_{n+1}

$$\mathbf{S}_{n+1} = \mathbf{\Xi}(\Delta\gamma)\mathbf{D}^{-1}\mathbf{S}^{trial}_{n+1} \tag{3-40}$$

$$\alpha_{n+1} = \alpha_n + \Delta\gamma\sqrt{\frac{2}{3}}\sqrt{\mathbf{S}_{n+1}\mathbf{P}\mathbf{S}_{n+1}} \tag{3-41}$$

$$\mathbf{E}^{vp}_{n+1} = \mathbf{E}^{vp}_n + \Delta\gamma\mathbf{P}\mathbf{S}_{n+1} \tag{3-42}$$

5. Compute the consistent elastoviscoplastic tangent moduli

$$\Theta = \left[\frac{1}{K} - \sqrt{\frac{2}{3}}\frac{\partial\Delta\gamma}{\partial q}\left(\chi\mathbf{S}_{n+1}\mathbf{P} - \bar{f}\right)\right]^{-1} \tag{3-43}$$

$$\chi = \left(\frac{\Delta\gamma}{\bar{f}}\mathbf{S}_{n+1}\mathbf{P} + \bar{f}\frac{\partial\Delta\gamma}{\partial\mathbf{S}_{n+1}}\right)\mathbf{\Xi} \tag{3-44}$$

$$\left.\frac{d\mathbf{S}}{d\mathbf{E}}\right|_{n+1} = \mathbf{\Xi} + \mathbf{\Xi}\frac{\partial\Delta\gamma}{\partial q}\mathbf{S}_{n+1}\mathbf{P}\left(\Theta\sqrt{\frac{2}{3}}\chi\right) \tag{3-45}$$

6. Update E_{33}

$$E_{33n+1} = -\frac{\nu}{E}(S_{11n+1} + S_{22n+1}) - (E^{vp}_{11n+1} + E^{vp}_{22n+1}) \tag{3-46}$$

Box 3.3: Algorithm for the elastoviscoplastic material

In the present work the Perić model is used to describe $< f_{n+1} >$ (equation 3-34). This equation was rewritten in a more stable form, according to Perić apud Souza Neto et al. [40] as:

$$\phi(\Delta\gamma) = \left(\frac{\Delta t}{\Delta\gamma\mu + \Delta t}\right)^{\epsilon} \cdot \left(\frac{1}{2}\bar{f}^2\right) - \frac{1}{3}R^2 = 0 \tag{3-47}$$

Changes in the algorithm of the elastoplastic model, more precisely in equations 4 to 6, are introduced. Due to internal variables integration in time and to the viscoplastic parameter. This modified algorithm has the work of Simo and Govindjee [57] as basis and it is shown in box 3.3.

1. Set initial guess for $\Delta\gamma$

$$\Delta\gamma = 0$$

$$\phi(\Delta\gamma) = \left(\frac{\Delta t}{\Delta\gamma\mu + \Delta t}\right)^{\epsilon} \cdot \left(\frac{1}{2}\overline{f^2}\right) - \frac{1}{3}R^2 = 0 \tag{3-48}$$

2. Perform Newton-Raphson iteration

$$\overline{f'} = -\frac{1}{3}\frac{\left(S_{11}^{trial} + S_{22}^{trial}\right)^2 E}{\left(1 + \frac{E\Delta\gamma}{3-3\nu}\right)^3 (3 - 3\nu)} - \frac{\left(\left(S_{11}^{trial} - S_{22}^{trial}\right)^2 + 4S_{21}^{trial2}\right)E}{\left(1 + \frac{E\Delta\gamma}{1+\nu}\right)^3 (1 + \nu)} \tag{3-49}$$

$$R^{2'} = 2\sigma_y\left(\alpha_n + \Delta\gamma\sqrt{\frac{2}{3}\overline{f}}\right)K\sqrt{\frac{2}{3}}\left(\sqrt{\overline{f}} + \frac{\Delta\gamma\overline{f'}}{2\sqrt{\overline{f}}}\right) \tag{3-50}$$

$$\phi'(\Delta\gamma) = -\frac{\epsilon\mu}{\Delta\gamma\mu + \Delta t}\left(\frac{\Delta t}{\Delta\gamma\mu + \Delta t}\right)^{\epsilon} \cdot \frac{1}{2}\overline{f^2} + \left(\frac{\Delta t}{\Delta\gamma\mu + \Delta t}\right)^{\epsilon} \cdot \left(\frac{1}{2}\overline{f'}\right) - \frac{1}{3}R^{2'} \tag{3-51}$$

$$\Delta\gamma_{n+1} = \Delta\gamma_n - \frac{\phi}{\phi'} \tag{3-52}$$

3. Check for convergence if $\Delta\gamma_{n+1} - \Delta\gamma_n \leq tol$ then return to box 3.3 else go to 1

Box 3.4: Newton–Raphson algorithm to solve $\Delta\gamma$ including Perić model

3.2.3
Benchmark Example

The benchmark example of the viscoplastic material model implementation is the same presented in section 3.1.3 to validate the implementation of the elastoplastic material model. The problem consists of axial stretching at constant rate of a perforated rectangular strip with the same geometry, mesh, boundary conditions and the elastic and plastic material properties as in section 3.1.3. The viscosity parameter is $\mu = 500s$ and two values for the rate sensitivity are adopted $\epsilon = 1$ and 0.1.

The results for rate sensitivity of 1.0 and 0.1 are shown in figures 3.7(a) and 3.7(b), respectively.

The deformation rate is defined by:

$$\frac{v}{L} \tag{3-53}$$

where v is the stretching velocity imposed on the free edge and L is the length of the strip, which is 18 (see figure 3.4).

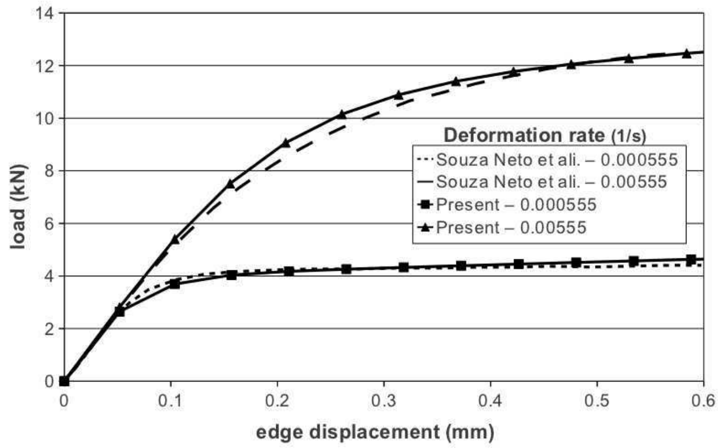

(a)

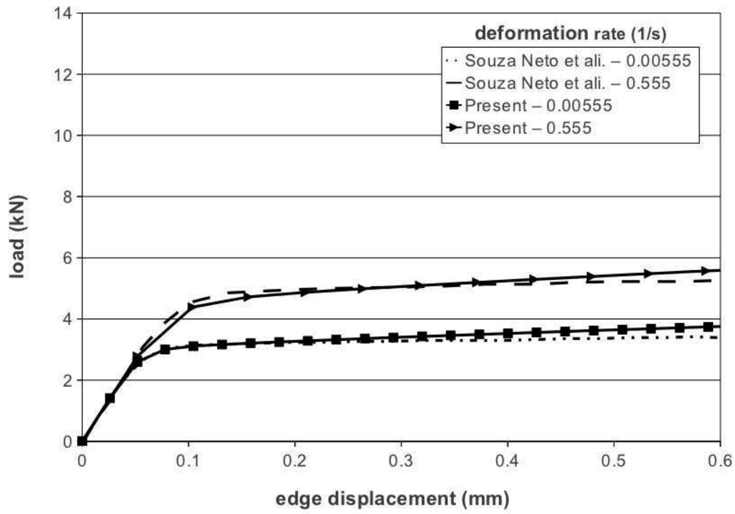

(b)

Figure 3.7: Force versus displacement curve of a perforated rectangular membrane: (a) $\epsilon = 1.0$ and (b) $\epsilon = 0.1$.

3.3
Large strains — Hyperelasticity

The theory of large strains or finite strains considers that both rotations and strains of a body are large. As the material of membranes usually present large strains, some material models with finite strains are implemented and presented in this section.

The hyperelasticity theory considers that a material has a nonlinear elastic response with large strains. A hyperelastic material is defined through a Helmholtz free-energy function (W), often named strain energy.

Some models with their respective strain energy functions follow.

3.3.1 Mooney–Rivlin model

The strain-energy function for the Mooney-Rivlin model is expressed by:

$$W(I_1, I_2) = C_1(I_1 - 3) + C_2(I_2 - 3) \tag{3-54}$$

where C_1 and C_2 are material constants and I_1 and I_2 are the first and the second stretch invariants given by:

$$I_1 = det(\mathbf{F})^{-2/3}\left(\lambda_1^2 + \lambda_2^2 + \lambda_3^2\right) \tag{3-55}$$

$$I_2 = det(\mathbf{F})^{-4/3}\left(\lambda_1^2\lambda_2^2 + \lambda_2^2\lambda_3^2 + \lambda_3^2\lambda_1^2\right) \tag{3-56}$$

3.3.2 Neo–Hookean model

The strain-energy function for the Neo-Hookean model is obtained from the Mooney-Rivlin model by setting $C_2 = 0$

$$W(I_1, I_2) = C_1(I_1 - 3) \tag{3-57}$$

3.3.3 Ogden model

The strain-energy for the Ogden model [58] is defined as:

$$W(\lambda_\gamma) = \sum_r \frac{\mu_r}{\alpha_r}[\lambda_1^{\alpha_r} + \lambda_2^{\alpha_r} + (\lambda_1\lambda_2)^{-\alpha_r} - 3], \qquad \gamma = 1, 2 \tag{3-58}$$

In the present work the Ogden material model ([59],[58]) is implemented, because it includes the special cases of the Neo-Hookean and the Mooney-Rivlin materials. This implementation is based on the work of Gruttmann and Taylor [60]. The formulation requires the computation and linearization of the principal stretches, which are the eigenvalues of the right stretch tensor $\mathbf{C}$.

In accordance with the deformation energy equation, the second Piola-Kirchhoff stress tensor is given by:

$$\mathbf{S}_\gamma = \lambda_\gamma^{-1}\frac{\partial W}{\partial \lambda_\gamma} = \lambda_\gamma^{-2}\sum_r \mu_r[\lambda_\gamma^{\alpha_r} - (\lambda_1\lambda_2)^{-\alpha_r}], \qquad \gamma = 1, 2 \tag{3-59}$$

The tangent material matrix, is determined:

$$\mathbf{C}_T = \mathbf{T}^T\bar{\mathbf{C}}\mathbf{T} = \begin{bmatrix} \frac{\partial S^{11}}{\partial E_{11}} & \frac{\partial S^{11}}{\partial E_{22}} & \frac{\partial S^{11}}{\partial 2E_{12}} \\ \frac{\partial S^{22}}{\partial E_{11}} & \frac{\partial S^{22}}{\partial E_{22}} & \frac{\partial S^{22}}{\partial 2E_{12}} \\ \frac{\partial S^{12}}{\partial E_{11}} & \frac{\partial S^{12}}{\partial E_{22}} & \frac{\partial S^{12}}{\partial 2E_{12}} \end{bmatrix} \tag{3-60}$$

where:

$$\bar{\mathbf{C}} = \begin{bmatrix} \lambda_1^{-4}\left(\lambda_1\frac{\partial S_1}{\partial\lambda_1} - 2S_1\right) & \lambda_1^{-2}\lambda_2^{-2}\left(\lambda_2\frac{\partial S_1}{\partial\lambda_2}\right) & 0 \\ \lambda_1^{-2}\lambda_2^{-2}\left(\lambda_1\frac{\partial S_2}{\partial\lambda_1}\right) & \lambda_2^{-4}\left(\lambda_2\frac{\partial S_2}{\partial\lambda_2} - 2S_2\right) & 0 \\ 0 & 0 & \frac{(S_1-S_2)\cos(2\phi)}{C_{11}-C_{22}} \end{bmatrix} \tag{3-61}$$

$$T = \begin{bmatrix} cos^2\phi & sin^2\phi & cos\phi sin\phi \\ sin^2\phi & cos^2\phi & -cos\phi sin\phi \\ -2cos\phi sin\phi & 2cos\phi sin\phi & cos^2\phi - sin^2\phi \end{bmatrix} \tag{3-62}$$

$$S_\gamma = \lambda_\gamma^2 S_\gamma = \sum_r \mu_r[\lambda_\gamma^{\alpha_r} - (\lambda_1\lambda_2)^{-\alpha_r}], \qquad \gamma = 1, 2 \tag{3-63}$$

$$\lambda_1\frac{\partial S_1}{\partial\lambda_1} = \sum_r \mu_r\alpha_r[\lambda_1^{\alpha_r} + (\lambda_1\lambda_2)^{-\alpha_r}] \tag{3-64}$$

$$\lambda_2\frac{\partial S_2}{\partial\lambda_2} = \sum_r \mu_r\alpha_r[\lambda_2^{\alpha_r} + (\lambda_1\lambda_2)^{-\alpha_r}] \tag{3-65}$$

$$\lambda_2\frac{\partial S_1}{\partial\lambda_2} = \lambda_1\frac{\partial S_2}{\partial\lambda_1} = \sum_r \mu_r\alpha_r[(\lambda_1\lambda_2)^{-\alpha_r}] \tag{3-66}$$

3.3.4
Benchmark Example

To validate the implementation of the hyperelastic material model, a benchmark example is presented, which consists of the stretching of a square sheet with a circular hole. This example is found in Gruttmann and Taylor [60] and in Souza Neto et al. [40]. The length of the square is $20m$, the radius of the circle is $3m$ and the thickness is $1m$. Due to the symmetry, one quarter of the sheet was analyzed and the mesh with 200 linear quadrilateral membrane elements and 231 nodes is presented in figure 3.8(a). The material used is Mooney-Rivlin with the constant values of $C1 = 25MPa$ and $C2 = 7MPa$. Thus the Ogden material constants are $\mu_1 = 50MPa$, $\mu_2 = -14MPa$ and $\alpha_1 = 2$, $\alpha_2 = -2$. The analysis was performed under load control conditions in three steps.

Figure 3.9 shows the load–displacement curve of three points on the mesh (A, B and C highlighted in figure 3.8) compared with the solution of Gruttmann and Taylor [60].

The results for strains and stresses are shown in figure 3.10. The results obtained with the present implementation are the same as the results of Gruttmann and Taylor [60].

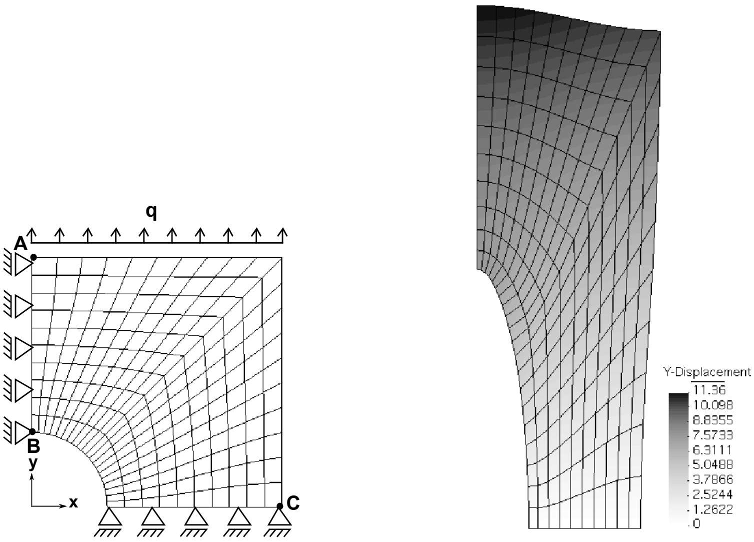

(a) (b)

Figure 3.8: Square sheet with a circular hole (a) undeformed sheet mesh with applied load (b) diplacement result in y direction with deformed sheet in a scale of 1:1.

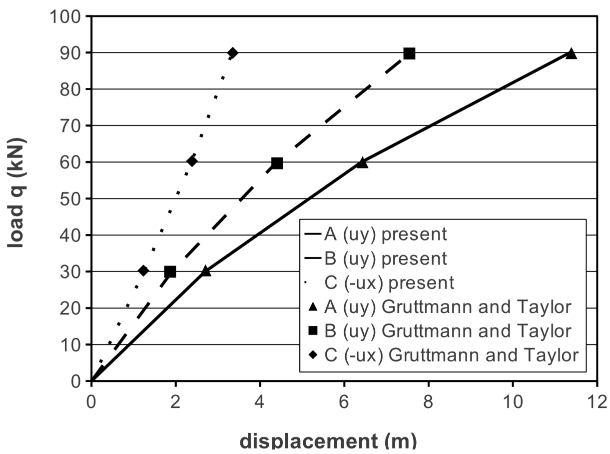

Figure 3.9: Load–displacement curves of stretching of a square sheet

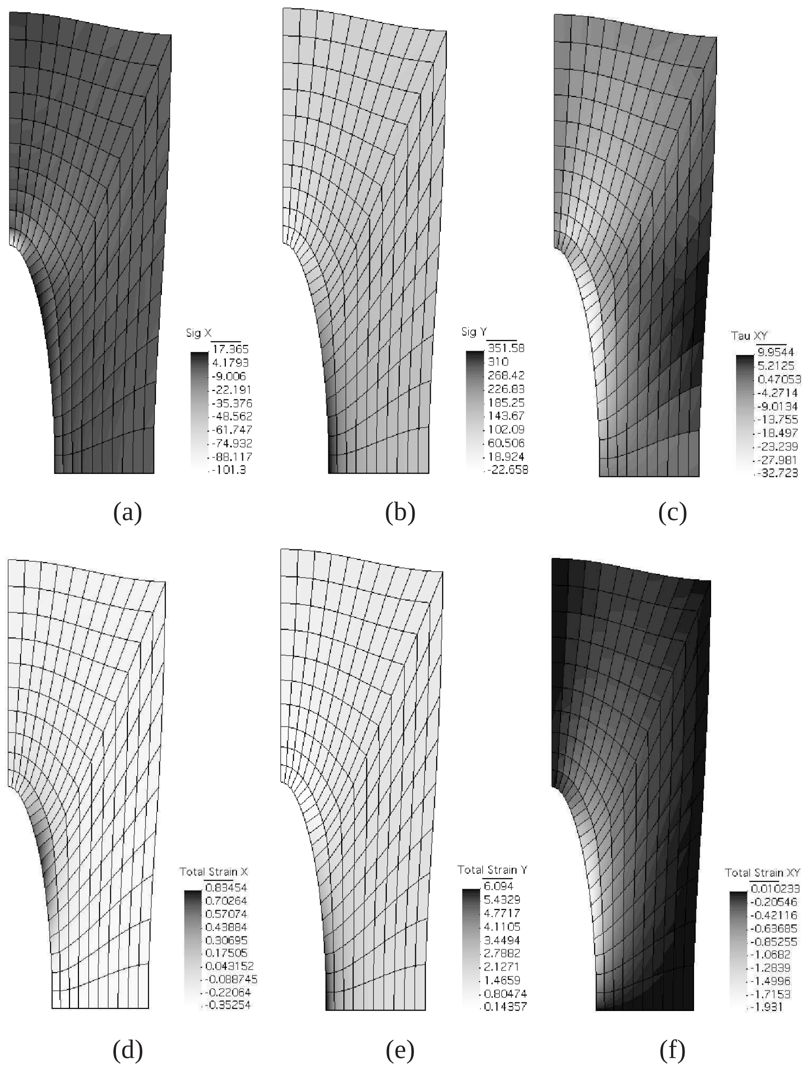

Figure 3.10: Results of the square sheet with a circular hole: (a) normal stress in x, (b) normal stress in y, (c) shear stress, (d) normal strain in x, (e) normal strain in y, and (f) shear strain

3.4 Large strains — Elastoplasticity

The multiplicative decomposition of the deformation gradient **F** is the main hypothesis in the finite strain elastoplasticity [38]. This hypothesis was introduced in chapter 2 in section 2.1 and it is here rewritten:

$$\mathbf{F} = \mathbf{F}^e\mathbf{F}^p$$

The implementation was carried out in this study preserving the return mapping schemes of the infinitesimal theory presented in section 3.1. Simo [42] showed that using Kirchhoff stress and logarithmic strain, the return mapping algorithm takes a format identical to the standard return mapping algorithms for the infinitesimal theory.

Taking the assumptions described above the implementation for elastoplasticity with large strains are summarized in box 3.5.

Souza Neto et al. [40] emphasizes that the simplicity of the integration algorithm of box 3.5 comes as a result of the assumptions of elastoplastic isotropy and the particular implicit exponential approximation adopted to discretise the plastic flow rule.

The present implementation is carried out based on the works of Perić et al. [61] and Caminero et al. [62] that present an algorithm for the total Lagrangian formulation. Caminero et al. [62] developed the large strain theory for anisotropic elastoplastic material for total and updated Lagrangian formulation. As isotropy is a particular case of anisotropy, this formulation can be used in the present implementation. Both works present a model for finite strains based on logarithmic strains.

The logarithmic strain measure and the Kirchhoff stress in Lagrangian description was introduced in chapter 2 in sections 2.2 and 2.3.

The numerical integration of the elastoplastic model is carried out with the elastic predictor and the plastic corrector scheme. The elastic predictor is calculated based on the multiplicative decomposition presented in equation 2-2 considering $\mathbf{F}^{p}_{n+1} = \mathbf{F}^{p}_{n}$, the trial elastic deformation gradient is given by:

$$\mathbf{F}^{e^{trial}}_{n+1} = \mathbf{F}_{n+1}\mathbf{F}^{p^{-1}}_{n+1} \tag{3-67}$$

The logarithmic trial strain is calculated with equation 2-12 and the Kirchhoff trial stress with the relation:

$$\mathbf{T}^{e^{trial}}_{n+1} = \mathbf{D}\mathbf{E}^{e^{trial}}_{L\,n+1} \tag{3-68}$$

where $\mathbf{D}$ is the elastic constitutive matrix presented in equation 3-20.

With the Kirchhoff trial stress the plastic corrector is calculated with the algorithm for small strains presented in box 3.2 and the Kirchhoff stress $\mathbf{T}_{n+1}$ and the plastic deformation gradient $\mathbf{F}^{p}_{n+1}$ are updated. Finally the consistent elastoplastic tangent moduli is computed.

Simo [63] and Ibrahimbegović ([64],[65]) computed the elastoplastic tangent moduli in spatial description. In the present work the elastoplastic tangent moduli is considered in material description.

The consistent elastoplastic tangent moduli $\frac{\partial \mathbf{S}}{\partial \mathbf{E}}$ is computed from the following equation:

$$\mathbf{S} = \mathbf{F}^{-1}\boldsymbol{\tau}\mathbf{F}^{-T} = \mathbf{F}^{-1}\mathbf{R}^{-T}\boldsymbol{\tau}\mathbf{R}^{-1}\mathbf{F}^{-T} \tag{3-69}$$

After some rearrangement and the symmetric tensor property $\mathbf{U} = \mathbf{U}^T$, equation 3-69 is rewritten:

$$\mathbf{S} = \mathbf{U}^{-1}\mathbf{T}\mathbf{U}^{-1} \rightarrow \mathbf{S}_{ij} = \mathbf{U}^{-1}_{im}\mathbf{T}_{mn}\mathbf{U}^{-1}_{nj} \tag{3-70}$$

The forth-order tensor $\frac{d\mathbf{S}}{d\mathbf{E}}$ can be written as:

$$\frac{\partial \mathbf{S}}{\partial \mathbf{E}} = \frac{\partial \mathbf{S}}{\partial \mathbf{C}}\frac{\partial \mathbf{C}}{\partial \mathbf{E}} = 2\frac{\partial \mathbf{S}}{\partial \mathbf{C}} \qquad \mathbf{E} = \frac{1}{2}(\mathbf{C} - \mathbf{I}) \tag{3-71}$$

The derivative of equation 3-69 w.r.t $\mathbf{C}_{kl}$ is given by:

$$2\frac{\partial \mathbf{S}_{ij}}{\partial \mathbf{C}_{kl}} = 2\left(\frac{\partial \mathbf{U}^{-1}_{im}}{\partial \mathbf{C}_{kl}}\mathbf{T}_{mn}\mathbf{U}^{-1}_{nj} + \mathbf{U}^{-1}_{im}\frac{\partial \mathbf{T}_{mn}}{\partial \mathbf{C}_{kl}}\mathbf{U}^{-1}_{nj} + \mathbf{U}^{-1}_{im}\mathbf{T}_{mn}\frac{\partial \mathbf{U}^{-1}_{nj}}{\partial \mathbf{C}_{kl}}\right) \tag{3-72}$$

The fourth-order tensor $\frac{\partial \mathbf{U}^{-1}_{im}}{\partial \mathbf{C}_{kl}}$ is computed applying the chain rule:

$$\frac{\partial \mathbf{U}^{-1}_{im}}{\partial \mathbf{C}_{kl}} = \frac{\partial \mathbf{U}^{-1}_{im}}{\partial \mathbf{U}_{pq}}\frac{\partial \mathbf{U}_{pq}}{\partial \mathbf{C}_{kl}} \tag{3-73}$$

where $\frac{\partial \mathbf{U}^{-1}_{im}}{\partial \mathbf{U}_{pq}}$ and $\frac{\partial \mathbf{U}_{pq}}{\partial \mathbf{C}_{kl}}$ according to Jog [66, 67] are given by:

$$\frac{\partial \mathbf{U}^{-1}}{\partial \mathbf{U}} = -\mathbf{U}^{-1} \boxtimes \mathbf{U}^{-1} \qquad \frac{\partial \mathbf{U}}{\partial \mathbf{C}} = [(\mathbf{U} \boxtimes \mathbf{I}) + (\mathbf{I} \boxtimes \mathbf{U})]^{-1} \tag{3-74}$$

where $\mathbf{A} \boxtimes \mathbf{B} = \mathbf{A}_{ik}\mathbf{B}_{jl}$, is defined by Jog [66].

The fourth-order tensor $\frac{\partial \mathbf{T}_{mn}}{\partial \mathbf{C}_{kl}}$ is also computed applying the chain rule:

$$\frac{\partial \mathbf{T}_{mn}}{\partial \mathbf{C}_{kl}} = \frac{\partial \mathbf{T}_{mn}}{\partial \mathbf{E}_{L\,pq}}\frac{\partial \mathbf{E}_{L\,pq}}{\partial \mathbf{C}_{kl}} \tag{3-75}$$

where $\frac{\partial \mathbf{T}_{mn}}{\partial \mathbf{E}_{L\,pq}}$ is the consistent elastoplastic moduli for Kirchhoff stress and logarithmic strain and $\frac{\partial \mathbf{E}_{L\,pq}}{\partial \mathbf{C}_{kl}}$ is computed with the study of Jog [67]:

$$\frac{\partial \mathbf{E}_L}{\partial \mathbf{C}} = \frac{\frac{1}{2}\partial\, ln(\mathbf{C})}{\partial \mathbf{C}} = \frac{1}{2}\left(\sum_{i=1}^{k}\frac{1}{\lambda_i}\mathbf{P}_i \boxtimes \mathbf{P}_i^T + \sum_{i=1}^{k}\sum_{j=1}^{k}{}_{j\neq i}\frac{ln(\lambda_i) - ln(\lambda_j)}{\lambda_i - \lambda_j}\mathbf{P}_i \boxtimes \mathbf{P}_j^T\right) \tag{3-76}$$

Box 3.6 summarizes the algorithm to compute the consistent elastoplastic moduli with large strains.

1. Take the plastic deformation gradient for the last converged step

$$\mathbf{F}^p_{n+1} = \mathbf{F}^p_n$$

2. Compute $\mathbf{F}^e_{n+1}$, $\mathbf{C}^e_{n+1}$, $\mathbf{U}^{e^{trial}}_{n+1}$, $\mathbf{E}^{e^{trial}}_{n+1}$ and $\mathbf{T}^{trial}_{n+1}$:

$$\mathbf{F}^e_{n+1} = \mathbf{F}_{n+1}\mathbf{F}^{p^{-1}}{}_{n+1}$$

$$\mathbf{C}^e_{n+1} = \mathbf{F}^{e^T}_{n+1}\mathbf{F}^e_{n+1} \quad \mathbf{C}^e = \sum_{i=0}^{2} \lambda_i^2 \mathbf{M}_i \qquad i = 1, 2$$

$$\mathbf{U}^{e^{trial}}_{n+1} = \sum_{i=0}^{2} \lambda_i \mathbf{M}_i \qquad i = 1, 2$$

$$\mathbf{E}^{e^{trial}}_{L n+1} = ln(\mathbf{U}^e_{n+1}) = \frac{1}{2} ln(\mathbf{B}^{e^{trial}}_{n+1}) = \sum_{i=0}^{2} ln(\lambda_i)\mathbf{M}_i \qquad i = 1, 2$$

$$\mathbf{T}^{trial}_{n+1} = \mathbf{D}\mathbf{E}^{e^{trial}}_{L n+1}$$

3. Solve $f(\Delta\gamma) = 0$ for $\Delta\gamma$ using the Newton–Raphson method — go to box 3.2 for elastoplastic material or 3.4 for elastoviscoplastic material (change S to T) and update $\mathbf{T}_{n+1}$ and $\mathbf{E}^e_{L n+1}$

$$\mathbf{E}^e_{L n+1} = \sum_{i=0}^{2} E^e_{L i}\mathbf{M}_i \qquad i = 1, 2$$

4. Compute $\mathbf{F}^p_{n+1}$, $\mathbf{E}^e$, and $\mathbf{E}^p$

$$\mathbf{F}^p_{n+1} = \mathbf{F}^p_{n+1} exp(\Delta\gamma \mathbf{P}\mathbf{T}_{n+1})$$

$$\mathbf{E}^e = \frac{1}{2}(\mathbf{C} - \mathbf{C}^p) \quad \mathbf{C} = \mathbf{F}^T\mathbf{F} \quad \mathbf{C}^p = \mathbf{F}^{p^T}\mathbf{F}^p$$

$$\mathbf{E}^p = \mathbf{E} - \mathbf{E}^e$$

5. Compute the consistent elastoplastic tangent moduli $\frac{d\mathbf{S}_{n+1}}{d\mathbf{E}_{n+1}}$ — go to box 3.6

Box 3.5: Algorithm of elastoplastic material with large strain

1. Compute $\frac{\partial \mathbf{T}_{mn}}{\partial \mathbf{E}_{L\,pq}}$ throught the consistent elastoplastic moduli for small strains from box 3.1(elastoplastic) or 3.3(elastoviscoplastic)

2. Compute $\frac{\partial \mathbf{U}^{-1}}{\partial \mathbf{U}}$, $\frac{\partial \mathbf{U}}{\partial \mathbf{C}}$ and $\frac{1}{2}\frac{\partial ln(\mathbf{C})}{\partial}\mathbf{C}$

$$\frac{\partial \mathbf{U}^{-1}}{\partial \mathbf{U}} = -\mathbf{U}^{-1} \boxtimes \mathbf{U}^{-1} \qquad \frac{\partial \mathbf{U}}{\partial \mathbf{C}} = [(\mathbf{U} \boxtimes \mathbf{I}) + (\mathbf{I} \boxtimes \mathbf{U})]^{-1}$$

$$\frac{\frac{1}{2}\partial\, ln(\mathbf{C})}{\partial \mathbf{C}} = \frac{1}{2}\left(\sum_{i=1}^{k} \frac{1}{\lambda_i}\mathbf{P}_i \boxtimes \mathbf{P}_i^T + \sum_{i=1}^{k}\sum_{\substack{j=1 \\ j\neq i}}^{k} \frac{ln(\lambda_i) - ln(\lambda_j)}{\lambda_i - \lambda_j}\mathbf{P}_i \boxtimes \mathbf{P}_j^T\right)$$

3. Compute $\frac{\partial \mathbf{U}^{-1}}{\partial \mathbf{C}}$ and $\frac{\partial \mathbf{T}}{\partial \mathbf{C}}$

$$\frac{\partial \mathbf{U}^{-1}}{\partial \mathbf{C}} = \frac{\partial \mathbf{U}^{-1}}{\partial \mathbf{U}}\frac{\partial \mathbf{U}}{\partial \mathbf{C}} \qquad \frac{\partial \mathbf{T}}{\partial \mathbf{C}} = \frac{\partial \mathbf{T}}{\partial \mathbf{E}_L}\frac{\partial \mathbf{E}_L}{\partial \mathbf{C}}$$

4. The consistent elastoplastic moduli is finally obtained

$$\frac{\partial \mathbf{S}_{ij}}{\partial \mathbf{E}_{kl}} = 2\left(\frac{\partial \mathbf{U}^{-1}_{im}}{\partial \mathbf{C}_{kl}}\mathbf{T}_{mn}\mathbf{U}^{-1}_{nj} + \mathbf{U}^{-1}_{im}\frac{\partial \mathbf{T}_{mn}}{\partial \mathbf{C}_{kl}}\mathbf{U}^{-1}_{nj} + \mathbf{U}^{-1}_{im}\mathbf{T}_{mn}\frac{\partial \mathbf{U}^{-1}_{nj}}{\partial \mathbf{C}_{kl}}\right)$$

Box 3.6: Algorithm for the consistent elastoplastic or elastoviscoplastic moduli

3.4.1 Benchmark Example

The benchmark example to validate the formulation implemented for the elastoplastic material with large strains is the same example presented in section 3.1.3 for the elastoplastic material with small strains. The problem consists of axial stretching at constant rate of a perforated rectangular strip whose geometry, mesh, boundary conditions, and material properties are common for both material behavior and are shown in section 3.1.3. The results obtained with the present implemented model, the small strains elastoplastic material model and the results of the literature (Souza Neto et al. [40]) are shown in figure 3.11.

The results obtained with the elastoplastic material model for large strains are in accordance with the results of the literature. The results of the elastoplastic material model for small strains are overestimated when the membrane starts to present large strains.

Figure 3.12 shows the stress versus strain curve for numerical analysis with large and small strains.

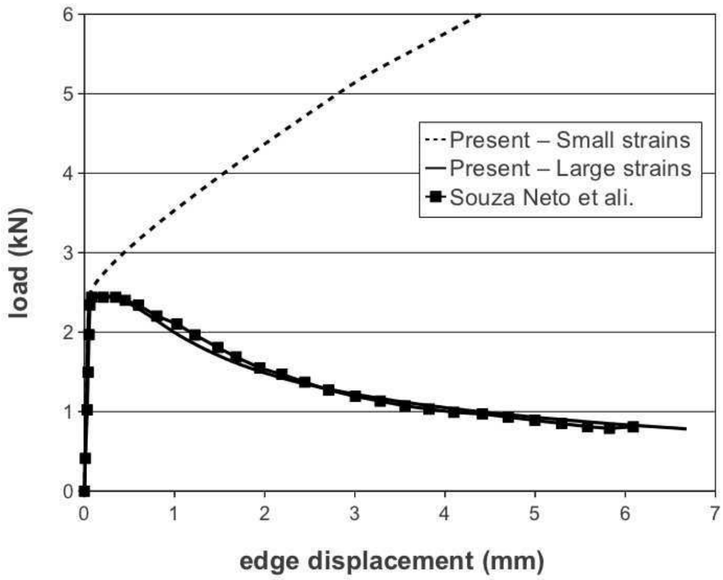

Figure 3.11: Force versus displacement on the free edge of a perforated rectangular membrane

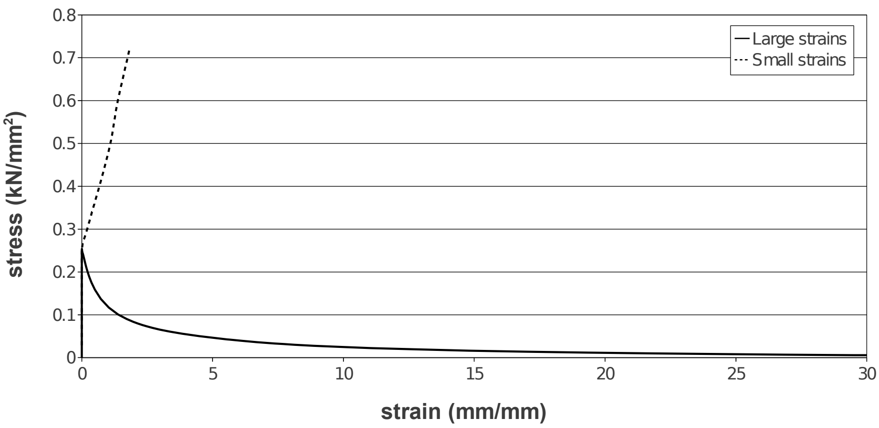

Figure 3.12: Stress versus strain for numerical analysis with large and small strains

3.5 Large strains — Elastoviscoplasticity

The present implementation of elastoviscoplastic material model with large strains is based on the concepts of elastoviscoplasticity with small strains presented in session 3.2 and the concepts of elastoplasticity with large strains presented in session 3.4. The implementation for this material is shown in box 3.5. The change for this material algorithm compared with the elastoplastic material model is the solution of $\Delta\gamma$ which is solved with box 3.4 and the constitutive material tensor $\frac{\partial \mathbf{T}_{mn}}{\partial \mathbf{E}_{L\,pq}}$ which is solved with box 3.3.

A reference work of elastoviscoplastic material model implementation with large strains is the work of Perić [68].